



**University of Dundee**

## **Polarised light sheet tomography**

Reidt, Sascha; O'Brien, Daniel; Wood, Kenneth; MacDonald, Michael

*Published in:*  
Optics Express

*DOI:*  
[10.1364/OE.24.011239](https://doi.org/10.1364/OE.24.011239)

*Publication date:*  
2016

*Document Version*  
Publisher's PDF, also known as Version of record

[Link to publication in Discovery Research Portal](#)

### *Citation for published version (APA):*

Reidt, S., O'Brien, D., Wood, K., & MacDonald, M. (2016). Polarised light sheet tomography. *Optics Express*, 24(10), 11239-11249. DOI: 10.1364/OE.24.011239

### **General rights**

Copyright and moral rights for the publications made accessible in Discovery Research Portal are retained by the authors and/or other copyright owners and it is a condition of accessing publications that users recognise and abide by the legal requirements associated with these rights.

- Users may download and print one copy of any publication from Discovery Research Portal for the purpose of private study or research.
- You may not further distribute the material or use it for any profit-making activity or commercial gain.
- You may freely distribute the URL identifying the publication in the public portal.

### **Take down policy**

If you believe that this document breaches copyright please contact us providing details, and we will remove access to the work immediately and investigate your claim.

# Polarised light sheet tomography

Sascha L. Reidt,<sup>1,3</sup> Daniel J. O'Brien,<sup>1,3</sup> Kenneth Wood,<sup>2</sup> and Michael P. MacDonald<sup>1,\*</sup>

<sup>1</sup>*Institute of Medical Science and Technology, University of Dundee, Mailbox 5 Level 6, Ninewells Hospital and Medical School, Dundee DD19SY, Scotland, UK*

<sup>2</sup>*School of Physics and Astronomy, University of St. Andrews, North Haugh, St. Andrews, Fife KY16 9SS, UK*

<sup>3</sup>*Authors contributed equally to this work*

\*[m.p.macdonald@dundee.ac.uk](mailto:m.p.macdonald@dundee.ac.uk)

**Abstract:** The various benefits of light sheet microscopy have made it a widely used modality for capturing three-dimensional images. It is mostly used for fluorescence imaging, but recently another technique called light sheet tomography solely relying on scattering was presented. The method was successfully applied to imaging of plant roots in transparent soil, but is limited when it comes to more turbid samples. This study presents a polarised light sheet tomography system and its advantages when imaging in highly scattering turbid media. The experimental configuration is guided by Monte Carlo radiation transfer methods, which model the propagation of a polarised light sheet in the sample. Images of both reflecting and absorbing phantoms in a complex collagenous matrix were acquired, and the results for different polarisation configurations are compared. Focus scanning methods were then used to reduce noise and produce three-dimensional reconstructions of absorbing targets.

©2016 Optical Society of America

**OCIS codes:** (110.0113) Imaging through turbid media; (170.6960) Tomography; (180.6900) Three-dimensional microscopy; (290.5855) Scattering, polarization.

---

## References and links

1. P. A. Santi, "Light sheet fluorescence microscopy: a review," *J. Histochem. Cytochem.* **59**(2), 129–138 (2011).
2. E. G. Reynaud, J. Peychl, J. Huisken, and P. Tomancak, "Guide to light-sheet microscopy for adventurous biologists," *Nat. Methods* **12**(1), 30–34 (2014).
3. J. Huisken, J. Swoger, F. Del Bene, J. Wittbrodt, and E. H. K. Stelzer, "Optical sectioning deep inside live embryos by selective plane illumination microscopy," *Science* **305**(5686), 1007–1009 (2004).
4. P. J. Keller, A. D. Schmidt, J. Wittbrodt, and E. H. K. Stelzer, "Reconstruction of zebrafish early embryonic development by scanned light sheet microscopy," *Science* **322**(5904), 1065–1069 (2008).
5. E. Rozbicki, M. Chuai, A. I. Karjalainen, F. Song, H. M. Sang, R. Martin, H.-J. Knölker, M. P. MacDonald, and C. J. Weijer, "Myosin-II-mediated cell shape changes and cell intercalation contribute to primitive streak formation," *Nat. Cell Biol.* **17**(4), 397–408 (2015).
6. A. Maizel, D. von Wangenheim, F. Federici, J. Haseloff, and E. H. Stelzer, "High-resolution live imaging of plant growth in near physiological bright conditions using light sheet fluorescence microscopy," *Plant J.* **68**(2), 377–385 (2011).
7. G. Sena, Z. Frentz, K. D. Birnbaum, and S. Leibler, "Quantitation of Cellular Dynamics in Growing Arabidopsis Roots with Light Sheet Microscopy," *PLoS One* **6**(6), e21303 (2011).
8. Y. Oshima, H. Sato, H. Kajiura-Kobayashi, T. Kimura, K. Naruse, and S. Nonaka, "Light sheet-excited spontaneous Raman imaging of a living fish by optical sectioning in a wide field Raman microscope," *Opt. Express* **20**(15), 16195–16204 (2012).
9. J. Mayer, A. Robert-Moreno, R. Danuser, J. V. Stein, J. Sharpe, and J. Swoger, "OPTiSPIM: integrating optical projection tomography in light sheet microscopy extends specimen characterization to nonfluorescent contrasts," *Opt. Lett.* **39**(4), 1053–1056 (2014).
10. A. Bassi, B. Schmid, and J. Huisken, "Optical tomography complements light sheet microscopy for *in toto* imaging of zebrafish development," *Development* **142**(5), 1016–1020 (2015).
11. Z. Yang, H. Downie, E. Rozbicki, L. X. Dupuy, and M. P. MacDonald, "Light Sheet Tomography (LST) for *in situ* imaging of plant roots," *Opt. Express* **21**(14), 16239–16247 (2013).
12. E. Berrocal, E. Kristensson, M. Richter, M. Linne, and M. Aldén, "Application of structured illumination for multiple scattering suppression in planar laser imaging of dense sprays," *Opt. Express* **16**(22), 17870–17881 (2008).

13. S. L. Jacques, J. R. Roman, and K. Lee, "Imaging superficial tissues with polarized light," *Lasers Surg. Med.* **26**(2), 119–129 (2000).
14. C. F. Bohren and D. R. Huffman, *Absorption and Scattering of Light by Small Particles* (John Wiley & Sons, 2008).
15. V. Backman, R. Gurjar, K. Badizadegan, I. Itzkan, R. R. Dasari, L. T. Perelman, and M. S. Feld, "Polarized light scattering spectroscopy for quantitative measurement of epithelial cellular structures in situ," *IEEE J. Sel. Top. Quantum Electron.* **5**(4), 1019–1026 (1999).
16. J. O'Doherty, J. Henricson, C. Anderson, M. J. Leahy, G. E. Nilsson, and F. Sjöberg, "Sub-epidermal imaging using polarized light spectroscopy for assessment of skin microcirculation," *Skin Res. Technol.* **13**(4), 472–484 (2007).
17. S. L. Jacques, J. C. Ramella-Roman, and K. Lee, "Imaging skin pathology with polarized light," *J. Biomed. Opt.* **7**(3), 329–340 (2002).
18. S. Saghafi, K. Becker, C. Hahn, and H. U. Dodt, "3D-ultramicroscopy utilizing aspheric optics," *J. Biophotonics* **7**(1-2), 117–125 (2014).
19. C. J. Engelbrecht and E. H. Stelzer, "Resolution enhancement in a light-sheet-based microscope (SPIM)," *Opt. Lett.* **31**(10), 1477–1479 (2006).
20. M. Shribak, S. Inoue, and R. Oldenbourg, "Polarization aberrations caused by differential transmission and phase shift in high-numerical-aperture lenses: theory, measurement, and rectification," *Opt. Eng.* **41**(5), 943–954 (2002).
21. A. D. Edelstein, M. A. Tsuchida, N. Amodaj, H. Pinkard, R. D. Vale, and N. Stuurman, "Advanced methods of microscope control using µManager software," *J. Biol. Methods* **1**(2), 10 (2014).
22. J. Schindelin, I. Arganda-Carreras, E. Frise, V. Kaynig, M. Longair, T. Pietzsch, S. Preibisch, C. Rueden, S. Saalfeld, B. Schmid, J. Y. Tinevez, D. J. White, V. Hartenstein, K. Eliceiri, P. Tomancak, and A. Cardona, "Fiji: An open-source platform for biological-image analysis," *Nat. Methods* **9**(7), 676–682 (2012).
23. J. Ramella-Roman, S. Prah, and S. Jacques, "Three Monte Carlo programs of polarized light transport into scattering media: part I," *Opt. Express* **13**(12), 4420–4438 (2005).
24. J. C. Ramella-Roman, S. A. Prah, and S. L. Jacques, "Three Monte Carlo programs of polarized light transport into scattering media: part II," *Opt. Express* **13**(25), 10392–10405 (2005).
25. B. A. Whitney, "Monte Carlo radiative transfer," *Bull. Astron. Soc. India* **39**, 101–127 (2011).
26. A. K. Glaser, Y. Wang, and J. T. C. Liu, "Assessing the imaging performance of light sheet microscopies in highly scattering tissues," *Biomed. Opt. Express* **7**(2), 454–466 (2016).
27. S. L. Jacques, "Optical properties of biological tissues: a review," *Phys. Med. Biol.* **58**(11), R37–R61 (2013).
28. P. Llull, X. Yuan, L. Carin, and D. J. Brady, "Image translation for single-shot focal tomography," *Optica* **2**(9), 822–825 (2015).
29. B. Forster, D. Van De Ville, J. Berent, D. Sage, and M. Unser, "Complex wavelets for extended depth-of-field: a new method for the fusion of multichannel microscopy images," *Microsc. Res. Tech.* **65**(1-2), 33–42 (2004).

## 1. Introduction

Single plane illumination microscopy, commonly termed 'light sheet microscopy' has received much attention in recent years by combining excellent spatio-temporal resolution with a large field of view and low photo-toxicity [1, 2]. For example, it is becoming widely used in developmental biology to image tissue dynamics of fluorescently labelled embryos [3–5] or to monitor plant growth [6, 7]. In this instance fluorophores are excited with a sheet of laser light and so the sample is optically sectioned. However, fluorescence is not an absolute requirement for light sheet microscopy as – in many cases – scattering can be used to obtain the necessary contrast. One such technique was developed to include Raman contrast in light sheet microscopy [8]. Another method relying on scattering, optical projection tomography, was also combined with light sheet microscopy in multimodal setups, computing images from projections to complement light sheet fluorescence images [9, 10]. In contrast, Light Sheet Tomography (LST) measures the scattered photons orthogonally to the illuminating laser light sheet. This compact and economical technique has been used to monitor the growth of plant roots in transparent soil [11] or in non-biological applications like structured planar laser imaging of dense sprays [12]. However, common to all light sheet techniques, images of more turbid samples are largely degraded by multiply scattered photons. As there are limited means of reconstructing the 'random walk' that these photons undergo, light sheet microscopy is still limited to samples with a low density of scattering objects.

In other optical imaging techniques for highly scattering samples this problem is addressed by utilising the polarisation aspect of light [13]. Photon polarisation not only

depends on the number of scattering events, but also on the nature of the scatterer encountered. On a microscopic level, scattering occurs when photons interact with a non-uniformity in the medium they are travelling through. This non-uniformity then results in a deviation of the photons travelling direction from its initial path. In media with a low density of scatterers, detection of the scattered photons allows localisation of the non-uniformity by simply back-projecting them along their direction of travel. In highly scattering media, a photon undergoes several of these scattering events before it can be detected, resulting in diffusion. The size of the object describes the scattering event as either Mie scattering, for scattering of particles with a diameter comparable to – or larger than – the wavelength of the photon, or by the Rayleigh approximation, for particles and molecules smaller than the wavelength of the photon. The resulting scattering angles depend on the type of scattering as well as on the polarisation of the photon. Typically, Mie scattering is highly anisotropic, with highly forward and backwards throwing scattering phase functions. Rayleigh scattering phase functions are more uniform, but the azimuthal angle highly depends on polarisation [14]. In the case of back-scattering, multiply scattered photons can be filtered in a cross-polarised configuration [15]. For example, polarisation spectroscopy was used for imaging in skin pathology by analysing the polarisation of back-scattered photons [16, 17].

In contrast to these techniques, this paper shows side-scattered photons imaged by a Polarised Light Sheet Tomography (PLST) system. A 3D Monte Carlo Radiation Transfer (MCRT) program simulates the scattering paths these photons may experience. MCRT also allows modelling of the orthogonal photon polarisation out of a propagating light sheet. The results of the simulations were validated experimentally by imaging targets immersed in complex and anisotropically scattering media. Furthermore the system is capable of noise reduction by continuous integration of sequential slices. This new PLST method shows a three-dimensional imaging technique to extract information from a turbid medium by using polarisation effects of orthogonally scattered light.

## 2. Materials and methods

### 2.1 Setup

The conversion of a LST system into a PLST system can be as straightforward as including polarising optics into the illumination pathway and analysing optics into the detection arm. This means the system can be prepared at a considerably low cost.

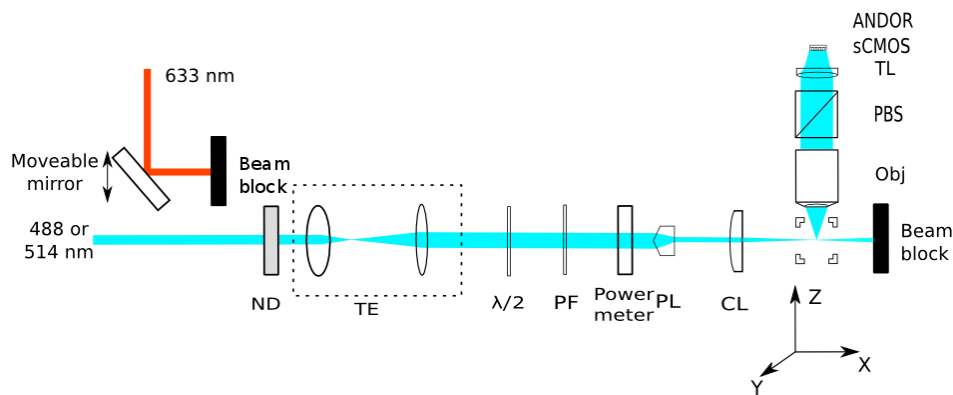


Fig. 1. Schematic of PLST setup (top view). ND-Neutral density filter, TE-Telescope, PF-Polarising filter, PL-Powell lens, CL-Cylindrical lens, Obj-Objective, PBS-Polarising Beam Splitter, TL-Tube lens.

The polarised light sheet tomography system, as shown in Fig. 1, was built with standard components. A He-Ne laser (JDS Uniphase 1136P) was used for illumination with 633 nm. A

multi-wavelength Ar-Ion laser (JDS Uniphase 2211-65MLQYV) was co-aligned with a removable mirror for illumination with 488 nm or 514 nm selected by appropriate filters. The chosen wavelengths allow co-registration of scattering particles and fluorescently labelled structures in future applications. The output beam was collimated by a telescope (Thorlabs LA1509  $f = 100\text{mm}$  and LA1229  $f = 175\text{mm}$ ). A zero-order half-wave plate (Thorlabs WPH10M-488) and a linear polarisation filter (Comar Optics 05 WL 25) were used to illuminate the sample with linearly polarised light and for power control, in addition to a set of neutral density filters (Thorlabs NEK01). As shown by Saghafi *et al.* [18] a uniform light sheet can be generated using a Powell lens. Here the light sheet was generated with two optical components; a Powell lens (Altechna 1-PL-1-B9101,  $10^\circ$  fan angle) combined with a cylindrical lens (Thorlabs LJ1212L1,  $f = 30\text{ mm}$ ). The samples were mounted on a motorised stage (three Physik Instrumente M111.12S). Deflected photons were collected by a 5x objective (Mitutoyo Plan Apo 5x /0.14) or a 10x objective (Mitutoyo Plan Apo 10x/0.28) orthogonal to the illumination plane. Such low NA optics are commonly used in lightsheet imaging, given that they provide a wide field of view without largely compromising axial resolution [19]. Their use in polarised light sheet tomography ensures that any depolarisation effects by the objectives are minimised [20]. In front of the tube lens (Thorlabs AC254-200-A-ML) and the camera (Andor Neo 5.5 sCMOS,  $2560 \times 2160$ ,  $6.5\ \mu\text{m}$  per pixel), a rotatable polarising beam splitter (Thorlabs CM1-PBS251) acted as a linear analyser in the detection axis. Note that the illumination laser and detection camera can easily be replaced by cheaper alternatives. The effective pixel size was found to be  $1.375\ \mu\text{m}$  and  $0.6875\ \mu\text{m}$  for the 5x and 10x objectives respectively. A power meter (Thorlabs PM100D with S121C head) was used to record power for each wavelength. A computer running Micro Manager [21] controlled the instruments and data was subsequently analysed in Fiji [22] and MATLAB. As depicted in Fig. 2, linear polarisation in the  $xz$ -plane is defined as parallel, while polarisation orthogonal to this, parallel to the  $y$ -axis, is defined as perpendicular.

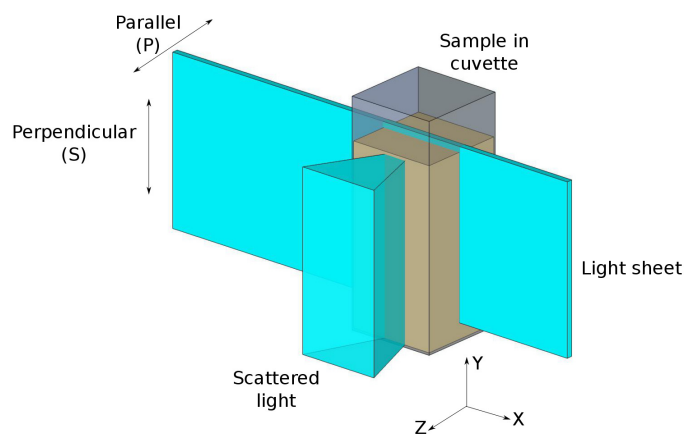


Fig. 2. Schematic describing the orientation of polarisation with respect to the light sheet. Linear polarisation in plane with the light sheet is described as perpendicular (s) polarised light, while light across the light sheet is described as parallel (p) polarised light.

## 2.2 Monte Carlo radiation transfer (MCRT) model

A 3D MCRT program was written in MATLAB for simulation of the light sheet tomography system. Photons were launched from a light sheet into a three-dimensional grid with predefined optical properties. The polarisation of the photons was modelled in the Stoke vector formalism with Mueller scattering matrices. Using a Lambertian model, internal diffuse reflection at boundaries between different media can be simulated. The scattering matrices for Mie scattering for a number of angles were precomputed numerically using code

written in C by Ramella-Roman [23, 24]. Rayleigh scattering parameters were computed analytically. In all cases, scattering angles were sampled with the rejection method. An azimuthal and a deflection angle are drawn from a uniform distribution, and the intensity of the potential scattering event is computed. The scattering angles are rejected and redrawn if the calculated intensity is smaller than a value randomly sampled from zero to the maximum of the intensity distribution. The photons are scattered until they get absorbed or leave the grid. The Stokes parameters of photons leaving the grid are captured, projected onto an image plane and filtered with virtual polarisers using Mueller matrices to model the imaging axis [25].

Before modelling the actual orthogonal scattering experiments, the newly developed MCRT code was tested by simulating a diffusion of polarisation experiment at a wavelength of 488 nm. A scattering medium in a three-dimensional cuboid was illuminated with a perfectly parallel-polarised beam of light. The non-absorbing medium consisted of an equal amount of Mie and Rayleigh scatterers with a total scattering coefficient of  $70 \text{ cm}^{-1}$ . The Mie scatterers were spheres with a diameter of  $2 \text{ }\mu\text{m}$  and showed a highly forward scattering behaviour, independent of polarisation. The Rayleigh phase function featured the typical side scattering, orthogonal to the plane of linear polarisation. The combination of both scattering types exhibited an anisotropy factor of 0.49, leading to a reduced scattering coefficient of  $34 \text{ cm}^{-1}$ . The lateral dimensions of the medium were kept constant at 0.5 mm. The thickness of the medium was increased step by step from 1 mean free path to 20 mean free paths, and the parallel-polarised component of the transmitted photons was measured as a function of the thickness in a total of 20 simulations. The result was fitted to the exponential decay postulated by Jacques *et al.* [13], showing a high r-squared value of 96.5%.

### 3. Results and discussion

#### 3.1 Light sheet generation

The beam shaping optics were chosen to overcome the issue of a somewhat elliptical beam profile, which occurs when using a cylindrical lens alone. A more uniform light sheet can be generated by implementing a Powell lens to redistribute the light into a fan, then focusing down in one axis with the cylindrical lens. The light sheet full width at half maximum generated with this combination was  $22 \text{ }\mu\text{m}$ , comparable to that formed using just the cylindrical lens. With the low NA of the cylindrical lens, the focus has a theoretical Rayleigh range of 0.56 mm. This is significantly larger than when using high NA optics for light sheet generation.

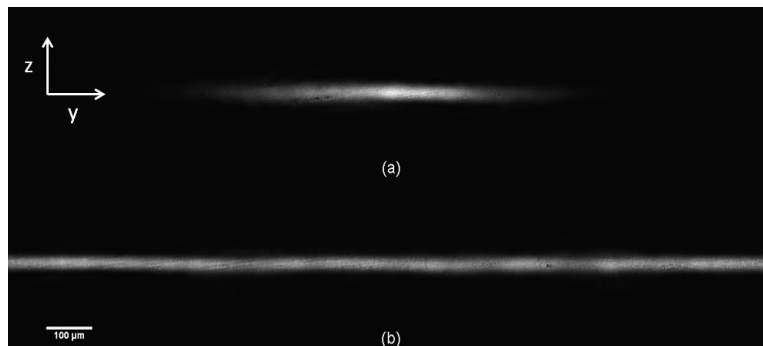


Fig. 3. Comparison of uniformity of (a) light sheet generated with just cylindrical lens and (b) light sheet generated using a combination of a Powell lens and cylindrical lens.

As shown in Fig. 3, the uniformity of the combined system is much greater than the cylindrical lens alone. This results in the intensity distribution being constant across the entire field of view. In contrast the light sheet created by just the cylindrical lens is largely Gaussian

across the field of view. In summary, this configuration is simple, uses off the shelf optics, and generates a thin uniform light sheet over a large field of view.

As in conventional light sheet microscopy the light sheet diffuses as it propagates in a scattering medium. The highly forward scattering nature of tissue increases the maximum depth at which satisfactory resolution can be achieved, which is in the range of 3-4 mean free paths, or about 300-400  $\mu\text{m}$  for generic human tissue [26]. The test media used in the following experiments were designed to exploit this limitation to show the merits of polarised detection over conventional means.

### 3.2 MCRT of a diffuse reflector in a scattering medium

The propagation of a polarised light sheet at 488 nm, with thickness of 20 $\mu\text{m}$ , was modelled with the MCRT program. As a target, a sphere with a diffuse reflection coefficient of 50% was immersed in the centre of a cube of a similar medium to that described above, with side lengths 0.5 mm and with a reduced scattering coefficient of 25  $\text{cm}^{-1}$  (compared for example to fibrous tissue with a mean value of 28  $\text{cm}^{-1}$  [27]). The sphere core was transparent, while the overall diameter was 100  $\mu\text{m}$ .

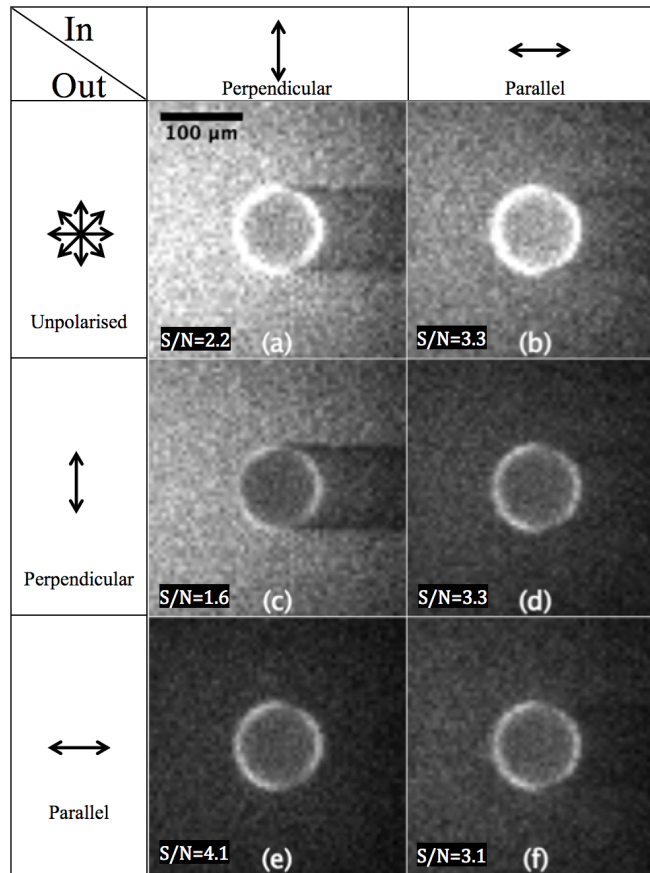


Fig. 4. Normalised MCRT results, with overlay values representing signal to noise ratio (S/N) as a figure-of-merit, showing perpendicular-polarised illumination (central column, vertical arrow) and parallel-polarised illumination (right column, horizontal arrow). Figure parts (a) perpendicular illumination with non-analysed detection, (b) parallel illumination with non-analysed detection, (c) perpendicular illumination with co-polarised detection, (d) parallel illumination with cross-polarised detection, (e) perpendicular illumination with cross-polarised detection and (f) parallel illumination with co-polarised detection.

The results of the simulation for different polarisations are shown in Fig. 4 with a normalised histogram. Signal to noise ratio was calculated for each simulation and is shown as a figure-of-merit in Fig. 4. These values were calculated by applying an annular mask over each sphere. A mean value was calculated both for this area and for a representative background signal with signal to noise ratio subsequently derived. The left column indicates that in the case of perpendicularly polarised illumination the noise level coming from the surrounding scattering medium is very high, due to the side-scattering nature of the Rayleigh scattering for this polarisation. Only in the case of a cross-polarised analysis in Fig. 4(e) does the signal coming from the reflecting shell appear to improve. On the right hand side, parallel illumination shows the target sharper and with a better signal to noise ratio, and the sphere can be imaged in the cross-polarised analysis of Fig. 4(d) or the co-polarised analysis of Fig. 4(f). The co-polarised detection has the advantage of a higher signal for the same illumination intensity.

### 3.3 Test samples

The PLST system was assessed using anisotropically scattering test materials. Images were recorded through Micro Manager. Analysis and reconstruction were performed in MATLAB and Fiji.

#### 3.3.1 Gelatine as a scattering medium

To make a highly scattering, complex medium, gelatine samples were prepared at 15% weight/volume in H<sub>2</sub>O, representing an anisotropic collagenous matrix. To increase the complexity of the scattering medium, 4% volume/volume of milk with 2% fatty acids was added to the gelatine. In a transmission experiment, the degree of polarisation decays as a function of the thickness of the medium, independent of the angle of the linear input polarisation. In an orthogonal scattering experiment however, the degree of polarisation of the output varies greatly with illumination polarisation. When illuminating the medium with parallel-polarised light at 488 nm, it was measured that only about 57% of the orthogonally scattered light is still parallel polarised. However, repeating the experiment with perpendicularly polarised illumination, the degree of polarisation was determined to be much higher, in the range of 73%. This shows that the perpendicular polarisation dominates when viewing orthogonally, and can be explained by the strongly side scattering nature of Rayleigh scattering for perpendicularly polarised light. This allows for contrast not normally accessible with co-axial detection.

#### 3.3.2 Polystyrene microspheres in gelatine

As reflectors with a known structure, 0.1 ml of 2.1% w/v 100 µm uniform polystyrene spheres in H<sub>2</sub>O solution (Thermo Scientific Dukes Standards 4310A) were imaged in 10% weight/volume gelatine. Images were normalised to the same intensity by adjusting the laser power to allow comparison of the polariser-analyser configurations.



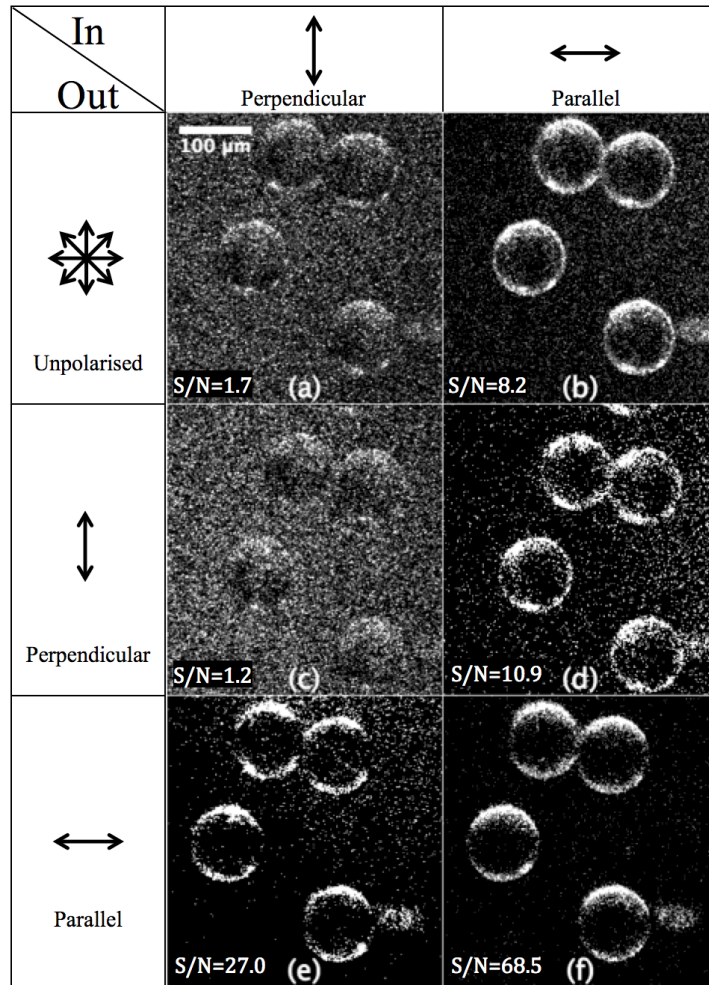


Fig. 5. 100  $\mu\text{m}$  scattering spheres in a 10% w/v gelatine medium, imaged with perpendicular-polarised illumination (central column, vertical arrow) and parallel-polarised illumination (right column, horizontal arrow), with overlay values representing signal to noise as a figure-of-merit. Figure parts (a) perpendicular illumination with non-analysed detection, (b) parallel illumination with non-analysed detection, (c) perpendicular illumination with co-polarised detection, (d) parallel illumination with cross-polarised detection, (e) perpendicular illumination with cross-polarised detection and (f) parallel illumination with co-polarised detection.

In Fig. 5, sections of the microsphere sample show four reflecting spheres immersed in the highly scattering gelatine-milk medium imaged at 488 nm for different polarisation configurations. Again signal to noise was derived as above. As with the MCRT simulations the left column shows images recorded with perpendicular illumination. They suffer from a high, speckled background noise coming from the higher orthogonal scattering levels of the medium. This speckle is not a consequence of polarisation, but of the coherent illumination. A means of reducing this speckle is discussed in Section 3.3.4. This background noise can be greatly reduced by using a cross-polarised detection regime as in Fig. 5(e), but this requires higher illumination intensity. The right column shows parallel illumination, with greatly improved results by using the co-polarised analysis in Fig. 5(f).

The experimental data, which concurs with the predictions of the Monte Carlo simulations, highlights the importance of polarisation control in such experiments. By using

parallel polarised illumination with co-polarised analysis, the microspheres that otherwise would be difficult to detect are revealed.

### 3.3.3 Polyurethane in gelatine

As another test to the system, commercially available polyurethane foam rubber was immersed in 15% weight per volume gelatine to create a phantom with a complex matrix structure. The foam rubber was chosen to be of a red colour, with equal absorption of 488 nm and 514 nm. Again, to increase the complexity of the scattering medium, 4% volume/volume milk with 2% fatty acids were added to the gelatine. Here, a stack of images, spaced at 10  $\mu\text{m}$ , was recorded at a constant power of 0.4 mW for the three different wavelengths: 488 nm, 514 nm and 633 nm.

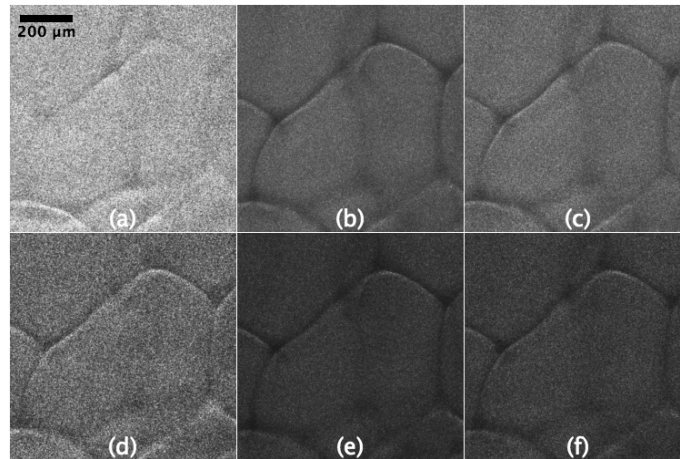


Fig. 6. Parallel illumination of the foam phantom with varying detection optics and colours. Each row represents a different detection of polarisation. Top row – unpolarised detection, (a) red channel, (b) green channel and (c) blue channel. Bottom row – co-polarised detection, (d) red channel, (e) green channel and (f) blue channel.

Figure 6 shows a representative section of the results from the foam in gelatine phantom. The absorbing strands can be seen for 488 nm and 514 nm, and the analyser improves image quality only slightly. The red light at 633 nm, which is reflected by the foam in image Fig. 6(a), benefits from the parallel co-polarised detection as shown in Fig. 6(d). By implementing the co-polarized detection regime the foam structure becomes visible. The choice of wavelengths adds another dimension to the method, and, given the large dependency of Rayleigh scattering on wavelength, some samples may benefit greatly from the use of a particular wavelength to increase contrast.

### 3.3.4 Noise reduction with focus scanning

Images as in Fig. 6 are influenced by high speckle noise levels, which translate to the three-dimensional stacks. Noise reduction can be achieved by deliberately blurring the image in a controlled manner [28]. This is done by capturing each image as the stage is moving continuously and results in an overall averaging of speckle. Here, the stage moved at a constant velocity of 0.25 mm/s with a set exposure time of 50 ms, resulting in each section being averaged over a distance of 12.5  $\mu\text{m}$ .

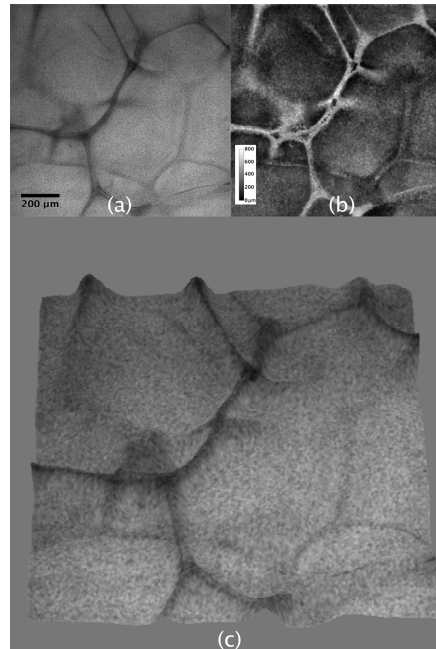


Fig. 7. (a) Axial projection, (b) topology and (c) three-dimensional extended depth of field reconstruction of foam phantom using parallel co-polarised optics.

By using a complex wavelet transform fusion algorithm [29], it is possible to use these intentionally blurred images to extract axial information from the data set acquired. The algorithm takes the in focus parts of each image and fuses them (in Fiji) to create one sharp composite image. Figure 7(a) shows the axial projection of the data stack acquired with 488 nm and Fig. 7(b) its topology, while Fig. 7(c) shows the resulting surface map of the foam phantom. The continuous scanning mean-filters the image stack in the z-dimension during acquisition, which improves image quality and increases the frame rate, but comes at the cost of slightly reduced axial resolution.

#### 4. Conclusion

Light sheet imaging is increasingly used in microscopy, especially in developmental biology and plant imaging. However, with increasing turbidity in samples, imaging becomes increasingly difficult. For light sheet tomography, 3D Monte Carlo Radiation Transfer simulations show that images can be greatly improved by controlling the polarisation of the illumination and of the analysis in the detection axis. Agreeing with this, the experimental image stacks acquired of reflecting targets immersed in a turbid medium suffer from a high noise level with the conventional light sheet tomography system, and adding polarisation optics greatly improves contrast and signal to noise ratio. More complicated, coloured targets like the strands of the polyurethane rubber were imaged with multiple wavelengths. The experimental data suggests that the improvement on the images by using PLST strongly depends on the wavelength and on the absorption spectrum of the sample. Samples with increasing complexity can be imaged by implementing the focus scanning method at the cost of axial resolution. This method allows the dynamic averaging of the images to reduce the noise, with shorter acquisition time and three-dimensional information accessible by computing surface plots.

This method extends a label free imaging technique into highly scattering samples, and remains compatible with fluorescence imaging. In addition, multi-wavelength PLST can be a useful tool for generating 3D composite images showing contrast mechanisms akin to

absorption spectra, or more complex phenomena like birefringence or wavelength dependence of Rayleigh scattering.

### **Acknowledgment**

The research leading to these results has received funding from the People Programme (Marie Curie Actions) of the European's Seventh Framework Programme (FP7/2007-2013) under REA grant agreement no. 608133 and Scottish Funding Council (SFC) Horizon fund. The authors sincerely thank both Dr. Craig McDougall and Dr. Paul O'Mahoney for their helpful insights and discussions that propelled this work to fruition.